AO14: Detection of Aircraft Emission Signatures in Atmospheric Spectra

Supervisors: Dr A. Dudhia, Dr C. Piccolo

Candidate Number: 26912

Abstract

Commercial jet aircraft are known to have both chemical and radiative impacts on the upper troposphere/lower stratosphere (UTLS), and with the aviation industry predicted to grow at a rate of 5% per year until at least 2015, a study of the impact of aircraft emissions is both relevant and important. Aircraft emissions are analysed and NO_2 is selected as the most suitable molecule for study. Model radiance spectra are generated using the MIPAS Reference Forward Model (RFM), before two-level retrieval methods are set up to detect a perturbation to the amount of NO_2 in the UTLS due to commercial jet aircraft, and MIPAS Aircraft Emission mode spectra are used in the retrievals. A linear retrieval method is shown to be inadequate, whilst a non-linear method is shown to be a potentially viable route for the detection of increased amounts of NO_2 in the UTLS and for further study.

1. Introduction

Commercial jet aircraft are known to have both chemical and radiative impacts on the upper troposphere/lower stratosphere (UTLS), the former through their direct injection of a variety of gases into this region of the atmosphere [1] and the latter through contrails seeding cirrus formation [2]. The aviation industry is projected to grow by about 5% per year until at least 2015 [3], whereas total aviation fuel use is projected to increase by 3% per year over the same period (the difference being due largely to improved aircraft efficiency) and so a study of the impact of aircraft engine emissions is highly relevant and also important, in order to predict the impact of a larger aircraft fleet.

The aim of this project is to attempt to detect and, if possible, quantify the chemical impact of commercial aircraft using infrared limb emission spectra obtained from the MIPAS satellite instrument on the European Space Agency's (ESA) Environmental Satellite (ENVISAT), concentrating on the North Atlantic corridor which has a high density of aircraft flights but is also relatively free from other anthropogenic influences. Satellite observations are the obvious means for monitoring the global chemical impact of aviation, yet even detecting aircraft emissions from space has proved challenging.

1.1 Aircraft Emissions

Table 1.1 shows the typical composition of aircraft emissions. The largest amounts of exhaust gases are released between 10km and 12km in altitude, corresponding to the most common aircraft cruising altitudes [4].

Molecule	Amount per kg of fuel	Background concentration at 12km (ppmv)
CO_2	3.15 kg	369
H_2O	1.26 kg	13.4
NO_x*	5-25 g	1.7×10^{-4}
CO	1-10 g	0.059
SO_2	< 1g	9.9×10^{-5}
Hydrocarbons	< 1g	-

Table 1.1 Typical composition of aircraft emissions, and typical background concentrations of each gas. *NO_x are oxides of nitrogen, defined as the sum of the amounts of nitric oxide (NO) and nitrogen dioxide (NO_2) with mass calculated as if the NO were in the form of NO_2

The current worldwide aircraft fleet produces only 2-3% of the total carbon dioxide (CO_2) released as a result of fossil fuel burning, and therefore only has a relatively small effect. Also, whilst CO_2 and water vapour (H_2O) make up the vast majority of aircraft emissions, neither current nor future subsonic aircraft emission rates will affect the ambient levels of these two molecules by more than a few percent [4]. Future supersonic aircraft, on the other hand, could perturb ambient H_2O levels significantly at their cruise altitudes, which lie in the stratosphere (supersonic cruise altitudes being several km higher than subsonic cruise altitudes for efficiency). The stratosphere is stable against vertical mixing, so pollutants introduced by man would take several years to be removed by transport and could therefore build up to globally damaging levels.

NO_x (NO_2 and NO) are the next most abundant molecules in aircraft emissions. High temperature

combustion in air leads to the formation of NO by 'fixing' of atmospheric N_2 and O_2, and the higher the temperature, the higher the NO emissions. Recent improvements in engine fuel efficiency (resulting in reduced CO_2 emissions) have come mainly from increasing engine combustion temperatures, which leads to increased NO_x emissions. Increased NO_x has an impact not only on air quality around airports, but also on climate change (see section 1.2). Typical NO_x concentrations in the UT are in the range 50-200 pptv [5], and personal communication from M. Köhler, University of Cambridge, showed zonally averaged increases of NO_x due to aircraft of up to 60 pptv are observed between 10 and 12 km.

CO emissions are of the same order of magnitude as NO_x emissions, although natural and non-aircraft anthropogenic sources of CO are substantially larger than analogous NO_x sources.

SO_2 is present in aircraft emissions to a lesser extent, and will be quickly converted to SO_3 or H_2SO_4 (Sulphuric Acid aerosol). Other minor constituents of aircraft emissions include HNO_3, N_2O_5 (an intermediate step between NO_2 and HNO_3), OH (which has no infrared emission signature), NO_3, HO_2NO_2 and HONO.

Based on the above, it was decided that several of the molecules in aircraft emissions might be worthy of further study: NO_2, NO, CO, HNO_3, NO_3, HO_2NO_2 and HONO. The radiative transfer model that was used throughout this project has no spectroscopic data for NO_3 or HONO, either reflecting that fact that these molecules have no infrared emission features or, more likely, that their naturally occurring concentrations are so small that their infrared absorption features are negligible for any practical purposes. The perturbations to the atmospheric spectra due to the other minor constituents (HNO_3 and HO_2NO_2) are so small that it is unlikely that they would be observable above the noise of the MIPAS instrument. NO is rapidly oxidised to form NO_2, and its infrared emission signature is much weaker than that of NO_2. The perturbations of CO and NO_2 due to aircraft are of similar magnitude, but as CO emits only in the MIPAS D band (see section 2), the band with poorest signal-to-noise ratio, it was decided that NO_2 would be the most appropriate molecule to investigate.

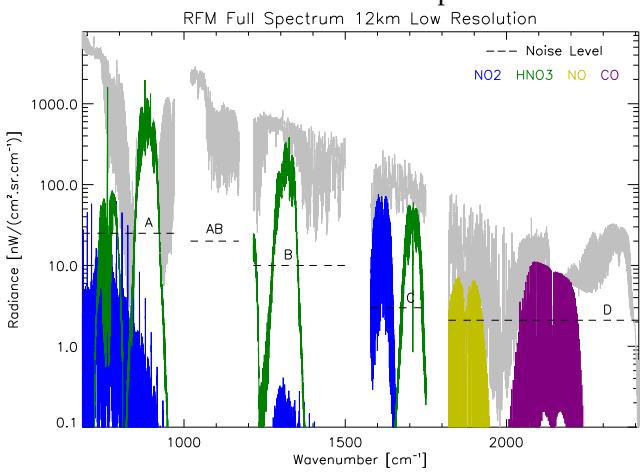

Figure 1.1 Model radiance spectrum simulated for a 12km tangent height. Radiance contributions of four molecules present in aircraft emissions are shown, along with the radiance from all emitting molecules in the atmosphere (grey line). The five MIPAS bands are labelled, together with the level of instrument noise in each band. Perturbations of CO and NO_2 due to aircraft are of similar magnitudes, but signal-to-noise ratio is better for NO_2.

1.2 NO_x Chemistry

NO and NO_2 are very influential in the chemistry of the troposphere and stratosphere, being important in ozone production and destruction and also the reduction in atmospheric lifetime and concentration of methane. Modification of the ozone layer would lead to changes in ultraviolet (UV) radiation reaching the Earth's surface. The response of O_3 to increased NO_x is negative (i.e. Ozone will decrease) in the middle stratosphere but positive below. An increase in the concentration of O_3 in the troposphere leads to radiative forcing, which in turn leads to warming of the Earth's surface and a reduction in the amount of UV-B reaching the surface. In the region where commercial aircraft fly, ozone is produced mainly from the oxidation of CO:

$$OH + CO \rightarrow H + CO_2 \quad (1.1)$$

$$H + O_2 + M \rightarrow HO_2 + M \quad (1.2)$$

$$HO_2 + NO \rightarrow NO_2 + OH \quad (1.3)$$

$$NO_2 + h\nu \rightarrow NO + O \quad (1.4)$$

$$O + O_2 + M \rightarrow O_3 + M \quad (1.5)$$

Net: $CO + 2O_2 \rightarrow CO_2 + O_3$

(M represents a gaseous third body such as N_2 or O_2)

The oxidation of CH_4 also contributes to ozone formation but is less important. The rates of these reactions depend directly on the concentrations of HO_x (OH and HO_2) and NO_x. Increases in the concentration of NO_x will generally increase the rate of ozone production by speeding the oxidation of CO and CH_4. In addition, NO_2 regulates the ozone budget via reactions with radicals to form reservoir species like HNO_3, $ClONO_2$, $BrONO_2$, and N_2O_5 which temporarily remove these radicals from fast ozone destroying reactions.

NO_2 exhibits a strong diurnal variation in the stratosphere [6], which is important in the context of this project, as the MIPAS instrument takes

measurements continuously. At sunset, NO is rapidly converted to NO_2 mainly via the reaction with O_3:

$$NO + O_3 \rightarrow NO_2 + O_2 \qquad (1.6)$$

During the night, NO_2 is gradually decomposed to form N_2O_5 by the following reactions:

$$NO_2 + O_3 \rightarrow NO_3 + O_2 \qquad (1.7)$$

$$NO_2 + NO_3 + M \rightarrow N_2O_5 + M \qquad (1.8)$$

After sunrise, N_2O_5 is photolysed back into NO_2 and NO_3 (or destroyed by collisional decomposition via the reverse reaction of equation (1.8)), and at the same time, NO_2 reacts very rapidly to reform NO either by photolysis or by reaction with atomic oxygen:

$$N_2O_5 + h\nu \rightarrow NO_2 + NO_3 \qquad (1.9)$$

$$NO_2 + h\nu \rightarrow NO + O(^3P) \qquad (1.10)$$

$$NO_2 + O \rightarrow NO + O_2 \qquad (1.11)$$

This diurnal variation of NO_2 results in a minimum stratospheric concentration after sunrise and a maximum stratospheric concentration shortly after sunset.

2 MIPAS

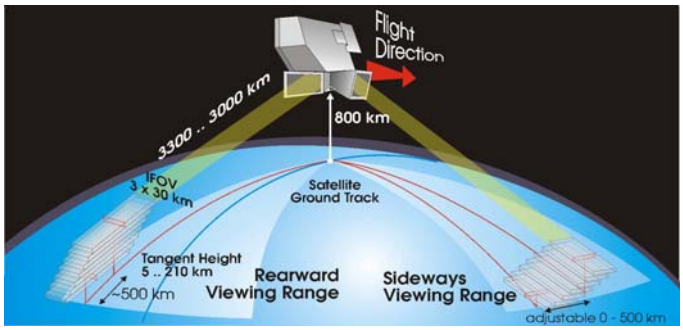

Figure 2.1 Image courtesy of the European Space Agency

In March 2002**,** the European Space Agency (ESA) launched their Environmental Satellite (ENVISAT), an advanced, polar-orbiting, Earth observation satellite, which provides measurements of the atmosphere, ocean, land, and ice from a height of 800km above the Earth. One of the instruments aboard ENVISAT is the Michelson Interferometer for Passive Atmospheric Sounding (MIPAS) (Figure 2.1), which is a Fourier transform spectrometer for the measurement of high-resolution gaseous emission spectra at the Earth's limb [7]. MIPAS observes the Earth's limb at about 3000km from the satellite, with a vertical resolution of 3km, coinciding with the vertical field of view (FOV) of 3km. It operates in the near to mid infrared (685cm^{-1} to 2410cm^{-1}, or 14.6μm – 4.15μm), where many of the atmospheric trace-gases playing a major role in atmospheric chemistry have important emission features. MIPAS can collect data from various altitudes and various positions by using two scanning mirrors to point at different angles to the side and to the rear of ENVISAT. This scanning capability combined with the orbit of ENVISAT allows MIPAS to achieve complete coverage of the Earth.

The spectrum measured by MIPAS is the result of the convolution of the instrument line shape (ILS) with the atmospheric spectrum entering the instrument. The ILS is similar to a sinc-function, and so has 'side lobes' decreasing linearly in amplitude, which means that the atmospheric signal at a given frequency affects the measured signal in a broad spectral interval. As a consequence of this, the forward model of a retrieval would have to consider spectral lines which are many wavenumbers away from the selected narrow spectral interval (microwindow). Convolution of the observations with an apodisation function reduces the amplitude of the side lobes of the ILS and accordingly the size of the spectral interval in which the atmospheric spectrum must be calculated, saving valuable computing time. The noise of the MIPAS instrument is better than 50$nW/cm^2.sr.cm^{-1}$, decreasing to 4.2$nW/cm^2.sr.cm^{-1}$ at the short wavelength side, and upon apodisation these values can be approximately halved.

2.1 Nominal Mode

For approximately 80% of the time MIPAS operates in its nominal mode, during which it routinely measures the atmospheric limb emission within a 35° wide range in the anti-flight direction (latitudinal resolution is increased by looking backwards), while the instrument's line-of-sight (LOS) is periodically varied in discrete steps. Up until March 2004 MIPAS operated in full resolution mode, with a spectral interval (the distance on the wavenumber axis between two consecutive spectral points) of 0.025cm^{-1}, and since then has been operating in reduced resolution mode, with a spectral interval of 0.0625cm^{-1}. Whilst in full resolution mode, the instrument's LOS was varied from a tangent height of 8km up to a tangent height of 68km in 3km steps. In reduced resolution mode, the LOS was altered and now varies between 6km and 70km, and MIPAS over samples the limb scan at low altitudes i.e. makes measurements at 1.5km tangent height spacing instead of the original 3km spacing. Also, in the reduced resolution mode, the instrument employs a "floating altitude grid", whereby the lowest LOS tangent altitude varies around the orbit, from approximately 5km over the poles to 12km over the equator. This is intended to approximately follow the shape of the tropopause to try

to maximise tropospheric coverage while minimising the number of spectra contaminated by cloud tops. At each height step, MIPAS records interferograms in five spectral bands, A: 685 - 970 cm^{-1}, AB: 1020 - 1170 cm^{-1}, B: 1215 - 1500 cm^{-1}, C: 1580 - 1750 cm^{-1}, and D: 1820 - 2410 cm^{-1}.

2.2 Aircraft Emissions Mode

For the remaining 20% measuring time MIPAS operates in one of a number of special modes, which involve the instrument pointing perpendicularly to the flight track in the anti-sun direction (i.e. in the range 80° to 110° from flight direction). This scanning geometry permits diurnal changes to be detected (see section 1.2) and specific geographic regions (such as Polar Regions in winter time) or special events (such as volcanic eruptions, or impact of aircraft) to be observed. In the Aircraft Emissions (AE) mode the line-of-sight is varied from a tangent height of 7km to 38km, in 1.5km steps, whilst interferograms are recorded over the region of the North Atlantic flight corridor, between latitudes of 34°N and 64°N and longitudes of +40° to -110°, in the same spectral bands as the MIPAS nominal mode. Figure 2.2 shows global MIPAS coverage for a single day, during which both nominal mode data and AE mode data were obtained.

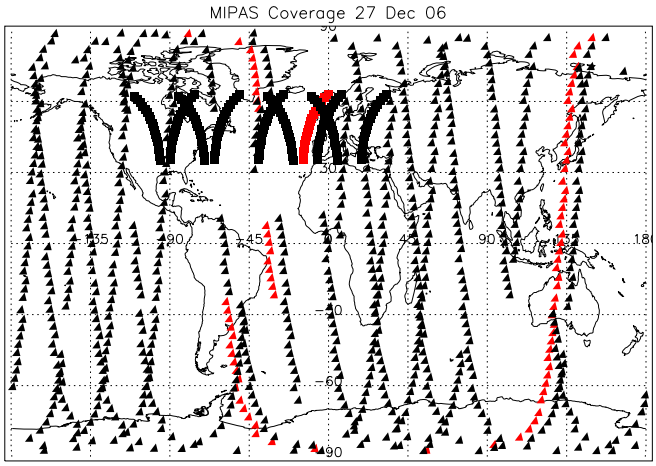

Figure 2.2 MIPAS coverage for 27/12/06. Nominal mode (rearward viewing) scans are depicted by triangles and Aircraft Emission mode (sideways viewing) scans are shown as squares. At each point interferograms are recorded over the whole line-of-sight altitude range. One complete orbit is highlighted in red, the start and end points of the orbit lying at the discontinuity at approximately 20°S.

Two main data products are obtained with MIPAS in all viewing modes: Level 1B - Radiometrically calibrated, spectrally corrected and geo-located spectra of radiance [9], and level 2 - Vertical profiles of pressure, temperature and volume mixing ratio (VMR) of O_3, H_2O, CH_4, N_2O, HNO_3 and NO_2 [10]. In this project I will be using only level 1B data.

3 Reference Forward Model (RFM)

The MIPAS RFM is a radiative transfer model which uses a given atmospheric profile and viewing geometry to generate simulated MIPAS spectra. Technical details on its operation can be found in reference [11]. The RFM is controlled using a driver table, which acts as a list of options, specifying exactly what the RFM is to process. A driver table containing all of the typical RFM details used in this project can be found in Appendix A.

Much computational time can be saved by running the RFM for only the relevant MIPAS bands and for only relevant tangent heights. It was found that NO_2 is present in MIPAS A, B and C bands, but has the greatest signal-to-noise ratio in the C band (see figure 1.1), where the NO_2 signal reaches almost 100nW and the band noise is 3nW.

Before the RFM is used to make model spectra, retrievals of pressure, temperature, and all relevant gases are conducted, in order that the model spectra will match the real spectra in all areas apart from the change under study. An example spectrum for typical mid-latitude conditions is shown in figure 3.1, the individual contributions to the radiance of various components being shown, as well as the total radiance. The

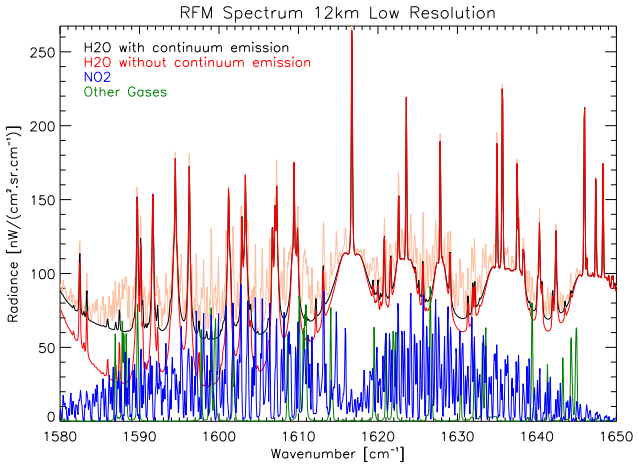

Figure 3.1 Typical RFM spectrum for the wavenumber region of highest NO_2 emission, showing contributions to the radiance from H_2O, NO_2 and all other gases. The total radiance is also shown (pink line)

wavenumber points most sensitive to a change in NO_2 are those where the NO_2 lines are largest relative to the total radiance. It is worth noting that the inclusion of the CTM flag in the RFM had a significant effect on the spectrum at tropospheric altitudes in the region of strongest NO_2 emission (1580-1610 cm^{-1}), showing that H_2O continuum emission is significant in the

troposphere in this region, despite there being a gap in the H_2O lines in this region.

4 Detectability of increased NO_2 concentration

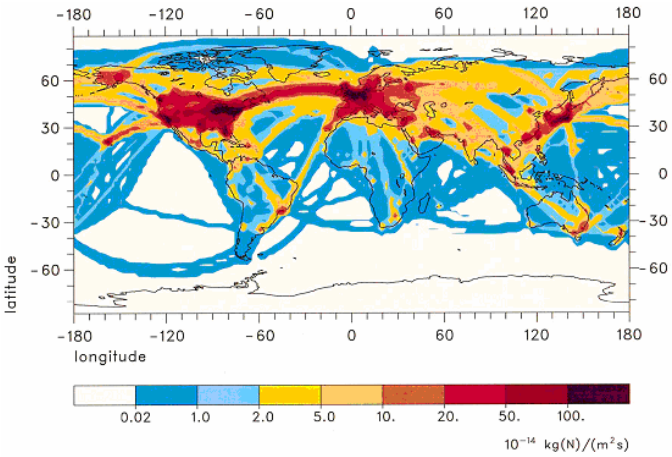

Figure 4.1 NO_x emissions by air traffic from ANCAT/EC2 inventory (annual mean) [12].

The first part of this project involved using the RFM to establish whether it is theoretically possible to detect an increased concentration of NO_2 due to aircraft, assuming that retrievals of temperature, pressure, H_2O, and all other relevant gases have been completed, so that the RFM spectra match the real atmospheric spectra.

In section 1, typical background NO_2 figures in the UT were quoted as 50-200 pptv, and zonally averaged increases of up to 60 pptv were said to be observed at altitudes of 10-12km. The majority of aircraft emissions in northern mid-latitudes can be found over North America, Europe and the North Atlantic (figure 4.1), and so it reasonable to assume that local increases of NO_2 levels in these regions could be double the zonally averaged value. The signal due to a 100% local enhancement in NO_2 at a 12km tangent height was calculated, and can be seen in figure 4.2. The highest points in the spectrum reach above the level of instrument noise, so in theory, detection of increased NO_2 due to aircraft would be possible at these points.

NO_2 is produced primarily in the lower stratosphere, from the oxidation of nitrous oxide (N_2O). As a result of this source, NO_2 concentrations in the lower stratosphere are quite large, reaching approximately 3000 pptv at an altitude of 20km [4], compared to a concentration of between 50 and 200 pptv at the tropopause. It is likely that variability of this high concentration of stratospheric NO_2 would mask increases in tropospheric NO_2 concentration when viewing from the limb, so in order to observe any increase it is necessary to consider a two-level retrieval, using measurements from two different tangent heights (Figure 4.3).

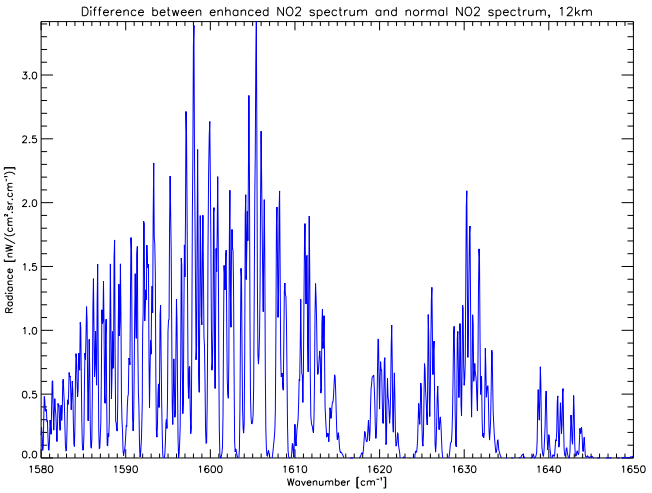

Figure 4.2 Signal produced at 12km tangent height for a 100% local increase in NO_2 concentration due to aircraft. The highest points in the spectrum reach above 3nW, the level of noise in the MIPAS C-band, so in theory, detection of increased NO_2 due to aircraft would be possible at these points

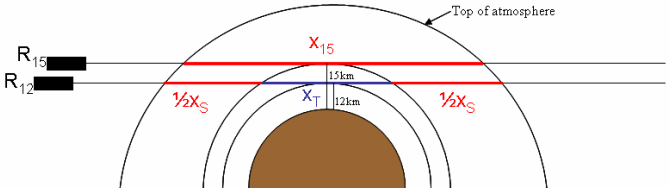

Figure 4.3 Two-level retrieval model. R_{12} and R_{15} represent the radiances received by MIPAS at the tropospheric and stratospheric levels respectively. x_n are the total number of NO_2 molecules in the horizontal path

4.1 Two-Level Linear Retrieval

Initially, a linear problem was assumed; radiance proportional to total number of molecules in the horizontal path.

$$R_{15} = ax_{15} \quad (4.1)$$

$$R_{12} = ax_{12} = a(x_T + x_S) \quad (4.2)$$

a = constant of proportionality, which approximately takes into account variations in atmospheric temperature.

A constant ratio of x_S the number of molecules in the stratosphere viewed at 12km tangent height, to x_{15}, the number of molecules in the stratosphere viewed at 15km tangent height, was assumed, the difference between these two figures arising from the geometry of the situation.

Combining equations 4.1 and 4.2 gives

$$\frac{R_{12}}{R_{15}} = \frac{x_S + x_T}{x_{15}} \qquad (4.3)$$

Algebraic manipulation gives the result

$$\frac{x_T}{x_S} = \frac{1}{b}\frac{R_{12}}{R_{15}} - 1, \qquad (4.4)$$

where $b = \frac{x_S}{x_{15}} = 0.771$, using figures computed by the RFM.

Ideally, a value of x_T, the tropospheric amount of NO_2, would be gained, but this is not possible with this set of equations. Values of x_T/x_S could still indicate an effect due to aircraft; if the ratio increases this implies an increase in the number of NO_2 molecules between 12km and 15km, relative to stratospheric amounts. Using horizontal path concentration values computed by the RFM, $x_T/x_S = 0.163$ in an atmosphere unperturbed by aircraft. In order to test the validity of the linear assumption, model radiance spectra were used in conjunction with equation 4.4 to calculate a set of values of x_T/x_S, one for each wavenumber point. If the linear case were exact, corresponding pairs of points on the model spectra would all give the same value of x_T/x_S, which would be equal to the value calculated above. The results are plotted in figure 4.4, the x-axis ranging from the wavenumber point of highest sensitivity to a change in NO_2, to the point of lowest sensitivity. Figure 4.4a shows the results for a model atmosphere containing all major infrared emitters, whilst figure 4.4b shows the results for an atmosphere consisting only of NO_2. In both cases, highly varying values of x_T/x_S can be seen at both wavenumbers of high sensitivity to NO_2 change and wavenumbers of low sensitivity, and all values are higher than the expected value, leading to the conclusion that a linear model is not a valid assumption.

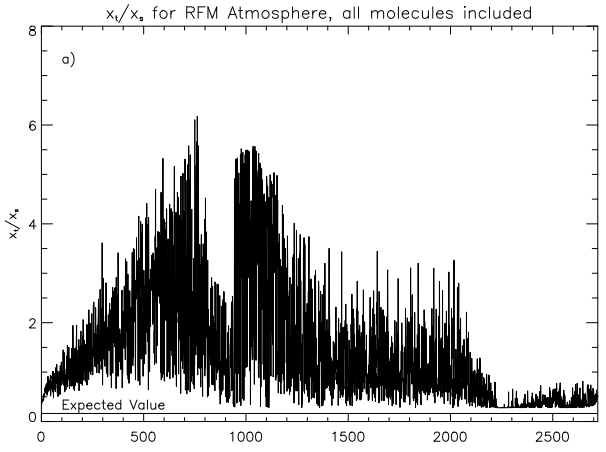

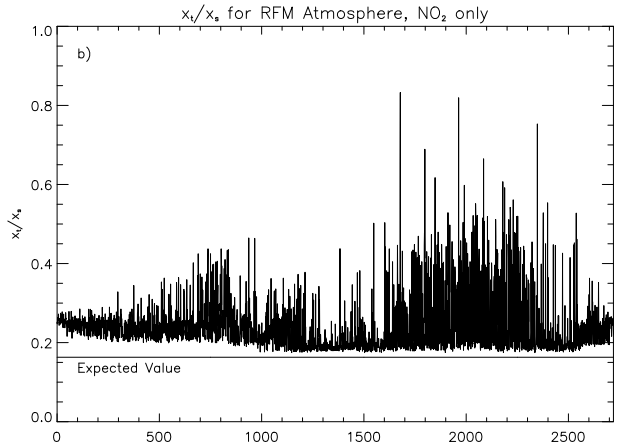

Figure 4.4 x_T/x_S values plotted from wavenumber points of high sensitivity to NO_2 change to wavenumber points of low sensitivity, for a) a model atmosphere containing all major infrared emitters and b) a model atmosphere consisting only of NO_2

4.2 Two-Level Non-Linear Retrieval

In reality, limb retrievals are generally non-linear, and so now, rather than assuming radiance is proportional to total number of molecules in the horizontal path, we say that radiance is some function of the number of molecules in the path. RFM spectra and MIPAS spectra will differ only by the additional radiance due to increased concentrations of NO_2, which is like a perturbation to the total radiance. Therefore, for a single tangent height we can write:

$$R_{12}^a - R_{12}^m = \left(\frac{\partial R_{12}}{\partial x_S}\right)\left(x_S^a - x_S^m\right) + \left(\frac{\partial R_{12}}{\partial x_T}\right)\left(x_T^a - x_T^m\right) \qquad (4.5)$$

R_{12}^a and R_{12}^m are the actual (MIPAS) radiance and model radiance values respectively.

$\left(\frac{\partial R_{12}}{\partial x_S}\right)$ is the RFM jacobian at 12km tangent height for a 1% increase in stratospheric NO_2

$\left(\frac{\partial R_{12}}{\partial x_T}\right)$ is the RFM jacobian at 12km tangent height for a 1% increase in tropospheric NO_2

x_S^a and x_S^m are the actual and model stratospheric concentrations of NO_2, and similarly, x_T^a and x_T^m are the actual and model tropospheric concentrations of NO_2. These values are expressed as percentages for simplicity, as the RFM jacobian is calculated for a 1% change. The values of model concentrations are taken to be 100% so that the real concentrations are expressed as a percentage of the model amount.

Similarly, for a 15km tangent height we can write

$$R_{15}^a - R_{15}^m = \left(\frac{\partial R_{15}}{\partial x_{15}}\right)\left(x_S^a - x_S^m\right) + \left(\frac{\partial R_{15}}{\partial x_T}\right)\left(x_T^a - x_T^m\right), \quad (4.6)$$

noting that in this case, the RFM jacobian at 15km tangent height for a 1% increase in tropospheric NO_2 will be equal to zero, due to the fact that we are observing at a level above the troposphere, and are therefore unable to notice any changes in tropospheric radiance.

Equations 4.5 and 4.6 can be combined to give

$$\begin{pmatrix} R_{15}^a - R_{15}^m \\ R_{12}^a - R_{12}^m \end{pmatrix} = \begin{pmatrix} \frac{\partial R_{15}}{\partial x_{15}} & \frac{\partial R_{15}}{\partial x_T} \\ \frac{\partial R_{12}}{\partial x_S} & \frac{\partial R_{12}}{\partial x_T} \end{pmatrix} \begin{pmatrix} x_S^a - x_S^m \\ x_T^a - x_T^m \end{pmatrix} \quad (4.7)$$

where $\underline{\mathbf{K}} = \begin{pmatrix} \frac{\partial R_{15}}{\partial x_{15}} & \frac{\partial R_{15}}{\partial x_T} \\ \frac{\partial R_{12}}{\partial x_S} & \frac{\partial R_{12}}{\partial x_T} \end{pmatrix}$

$\underline{\mathbf{K}}$ is known as the jacobian matrix, each element being made up of an RFM jacobian.

Letting $\underline{y} = \begin{pmatrix} R_{15}^a \\ R_{12}^a \end{pmatrix}$, $\underline{y}_m = \begin{pmatrix} R_{15}^m \\ R_{12}^m \end{pmatrix}$, $\underline{x} = \begin{pmatrix} x_S^a \\ x_T^a \end{pmatrix}$, and $\underline{x}_m = \begin{pmatrix} x_S^m \\ x_T^m \end{pmatrix} = \begin{pmatrix} 100 \\ 100 \end{pmatrix}$, equation 4.7 becomes

$$\underline{y} - \underline{y}_m = \underline{\mathbf{K}}\left(\underline{x} - \underline{x}_m\right) \quad (4.8)$$

Algebraic manipulation of 4.8 gives the result:

$$\underline{x} = \underline{x}_m + \underline{\mathbf{K}}^{-1}\left(\underline{y} - \underline{y}_m\right), \quad (4.9)$$

from which values of x_T (tropospheric NO_2 concentration as a percentage of the modelled concentration) can be gained, once RFM jacobians have been calculated.

5. Is detection of NO_2 perturbations possible in reality?

Four continuous days of MIPAS Aircraft Emissions (AE) mode data was available, from 26th-29th December 2006. Three consecutive days of data gives uniform longitudinal coverage due to a slight shift in orbital pattern each day, so data from 26th-28th December was used. In an ideal world, retrievals of temperature, pressure, and all relevant gases would already have been completed for each particular profile, and all RFM calculations would have been based on these. However, due to lack of time I'll start by looking for spectra which approximately match the mid-latitude conditions for which I have computed model spectra. The contributions of various gases to the emission spectrum in the region of strongest NO_2 emission can be seen in figure 3.1.

5.1 Cloud Detection

At low altitudes, in the troposphere, differences between modelled and MIPAS spectra could arise due to cloud. In the near to mid infrared, the spectral region in which MIPAS operates, cloud acts as a spectrally uniform emitter, which generally increases the radiance of gaseous emission lines, but simultaneously merges them with the background so that they become less distinguishable from it (see figure 5.1). In order to detect increased radiance due to increased tropospheric NO_2, it is necessary to be able to distinguish NO_2 emission lines from that of the continuum-like background, and so spectra contaminated with cloud need to be neglected.

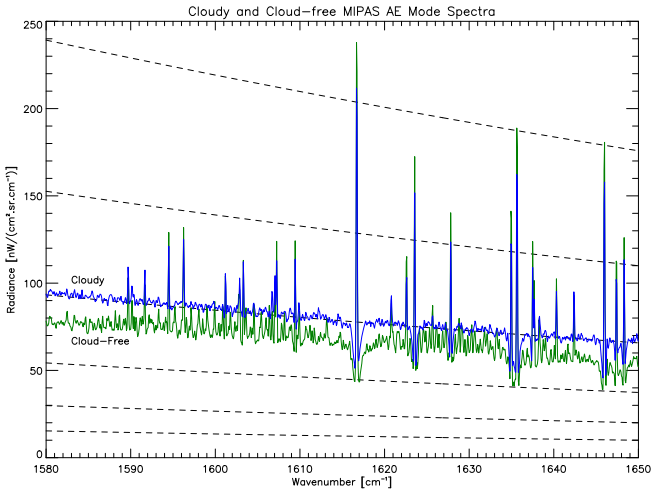

Figure 5.1 Plot showing the effect of cloud on MIPAS spectra. Radiance values are generally increased due to the presence of cloud, but emission lines gradually become less distinguishable from the background as cloud thickness increases. The dashed lines represent the Planck function at temperatures of 180K – 230K

The cloud detection algorithm designed for use with MIPAS [13], defines the Cloud Index (CI) as the ratio of mean radiances of two particular A-band microwindows, 788-796cm^{-1} (dominated by CO_2 and weak O_3 emissions) and 832-834cm^{-1} (where aerosols and cloud emissions, and some weak ozone and CFC11 emission lines are present). CI values are contained within MIPAS Level 1B data files; scans with a cloud index of less than 1.8 are taken to be cloudy.

Ideally, we would like to observe at tangent altitudes high enough to avoid cloud, enabling all

available MIPAS data to be used, but very few flights cruise above 13km which imposes an altitude limit.

5.2 Altitude Registration

Further differences between modelled and MIPAS spectra would be present if the tangent altitudes of MIPAS spectra were inaccurate. Altitude registration is particularly difficult for limb viewing spectrometers, as extremely small errors in the line-of-sight elevation angle result in large tangent altitude errors. Also, as MIPAS utilises both a rear-viewing mode and side-viewing mode, it is very sensitive to any changes in pitch or roll of the satellite/instrument system. A roll angle error of 42mdeg has been found [14], causing inaccurate tangent altitude values in the side-viewing (Aircraft Emission) mode. Such inaccuracies could be seen on comparison of nominal mode and AE mode spectra. Figure 5.2 shows MIPAS AE mode and nominal mode spectra from the same latitude and longitude – spectra at altitudes apparently over 3km apart look most similar to one another. Aircraft emission mode altitudes can be corrected, once level 2 processing of the data has taken place, using retrieved pressure and temperature values.

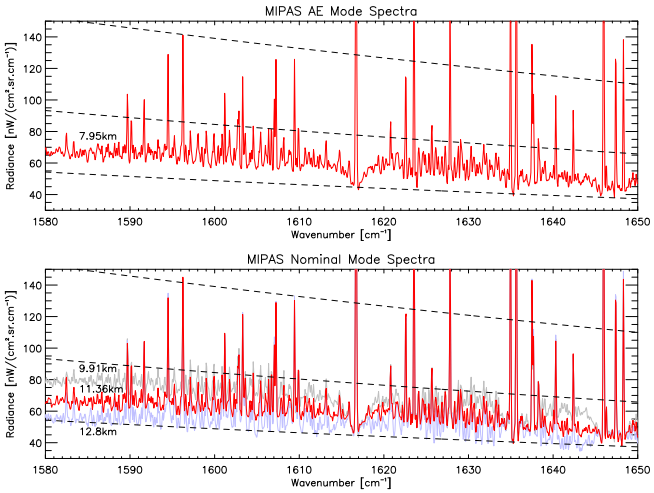

Figure 5.2 Comparison of MIPAS AE mode spectrum at an engineering (instrument measured), but incorrect, altitude of 7.95km with nominal mode spectra at three adjacent tangent altitudes: 9.91km, 11.38km and 12.80km. The AE spectrum looks most like the nominal mode spectrum at 11.38km, and this can be confirmed as the correct tangent height using retrieved tangent pressures

5.3 Spectra Matching

In order to have the best chance of detecting NO_2 perturbations, RFM spectra are required to match MIPAS spectra as closely as possible. A least squares approach was adopted to best fit the RFM spectra to the MIPAS spectra, which meant finding a scaling factor x that best fits the set of measurements in terms of minimising the square difference $\sum_i (y_i - m_i x)^2$, where y represents the real (MIPAS) spectra and m represents the model spectra. This is equivalent to minimising $(\mathbf{y}-\mathbf{m}x)^T(\mathbf{y}-\mathbf{m}x)$ as we vary x:

$$\frac{\partial}{\partial x}\left((\mathbf{y}-\mathbf{m}x)^T(\mathbf{y}-\mathbf{m}x)\right) = 0 \qquad (5.1)$$

$$-2\mathbf{m}^T(\mathbf{y}-\mathbf{m}x) = 0 \qquad (5.2)$$

$$-\mathbf{m}^T\mathbf{y}+\mathbf{m}^T\mathbf{m}x = 0 \qquad (5.3)$$

$$x = (\mathbf{m}^T\mathbf{m})^{-1}\mathbf{m}^T\mathbf{y} \qquad (5.4)$$

If using a perfect model, the model and real spectra would only differ by the noise, so the root-mean-squared (RMS) difference is equal to the noise. Therefore in the MIPAS C band, the best obtainable RMS difference is approximately 3nW. The minimum obtained using the mid-latitude RFM was 3.51nW.

The best lower level (tropospheric) fit was obtained using the mid-latitude RFM at 10.5km with nominal mode spectra at 12km and AE mode scans at a corrected altitude of 11.5km. Upper level (stratospheric) nominal mode spectra at 15km and AE mode spectra at 14.5km were most closely matched by model spectra at a tangent height of 11.5km. The root-mean-squared (RMS) differences between the model and MIPAS AE mode data are shown in figure 5.3. At both levels it could be seen that some of the MIPAS spectra matched the modelled spectra more closely than others, the anomalous spectra all lying over the western North Atlantic.

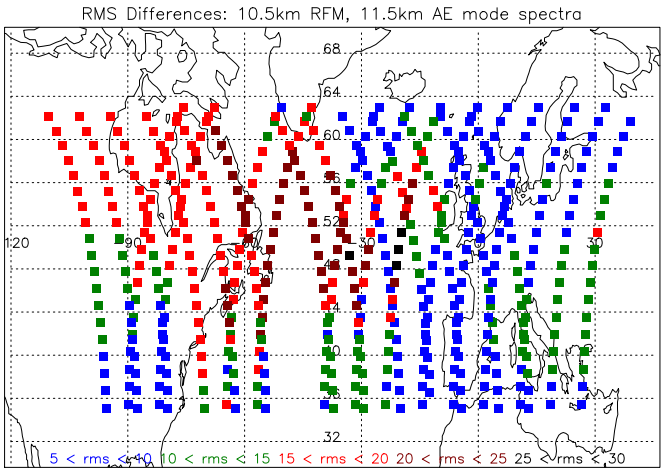

Figure 5.3 RMS differences between scaled RFM spectra and MIPAS AE mode spectra, showing a better match between modelled and MIPAS spectra in the east.

5.4 Meteorological Effects

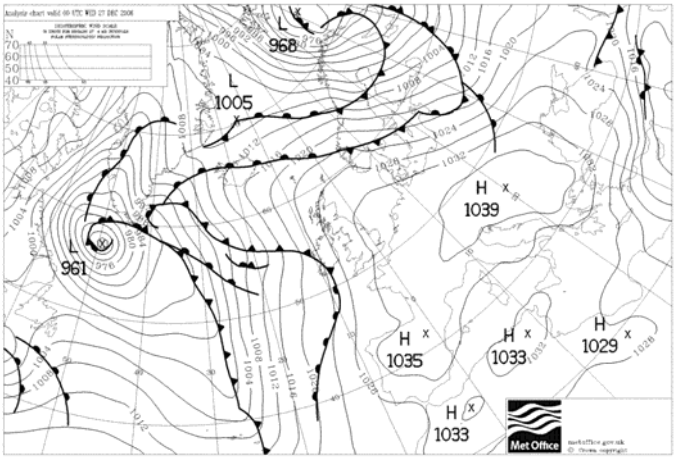

Figure 5.4 Synoptic Chart for 27/12/06 showing a low pressure system over the western North Atlantic; a possible cause of the anomalous MIPAS spectra in the same region

On inspection of synoptic charts (figure 5.4), a large, low pressure system could be seen moving west to east during the days that the MIPAS AE mode data was collected, which would bring polar air down towards the Western Atlantic coast, and could be the cause of the observed east-west divide. Polar winter conditions were modelled, and the models compared to MIPAS spectra, but they were found to be a poorer match than the mid-latitude models. Due to time constraints the cause of the anomalous spectra was not investigated further. Figure 5.5 shows the spectral differences between typical MIPAS spectra (over Europe and the eastern North Atlantic) and anomalous MIPAS spectra (over the western North Atlantic and North America), the differences being much the same for both cloudy and non-cloudy spectra.

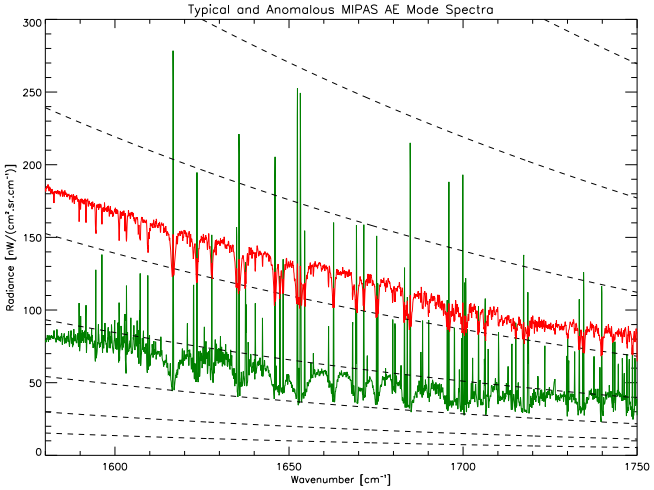

Figure 5.5 A typical MIPAS spectrum, found over Europe and the eastern North Atlantic (grey line), and an anomalous MIPAS spectrum, found over the western North Atlantic and North America (red line).

5.5 Linear Retrieval

Before any retrieval theory was applied, MIPAS spectra that couldn't be closely matched to model spectra (RMS difference greater than 15nW), and any cloudy spectra, were disregarded. Also, scans occurring close to sunrise and sunset were rejected due to the rapidly varying NO_2 concentration at these times (see section 1.2). The two-level linear retrieval theory described in section 4.1 was then applied to MIPAS spectra, in order to try to observe a general trend in x_T/x_S values over different latitudes and longitudes, although results were expected to be inaccurate for reasons discussed in section 4. It was hoped that higher values of x_T/x_S would be observed in general over the Northern hemisphere, as this is where the vast majority of NO_x emissions from aircraft can be found (see figure 4.1). The RFM was used to select the point in the spectrum most sensitive to a change in NO_2 (the wavenumber of the highest peak in the NO_2 jacobian spectrum), and the retrieval theory was applied at this single point (1605.44 cm^{-1}).

A value of x_T/x_S was retrieved for each MIPAS scan and a latitude-longitude plot of the values was produced, but the results were inconclusive.

5.6 Non-linear Retrieval

The more realistic two-level non-linear retrieval method described in section 4.2 was then applied to MIPAS spectra and values of x_T obtained for those scans for which the model and real data could be matched most closely (figure 5.6).

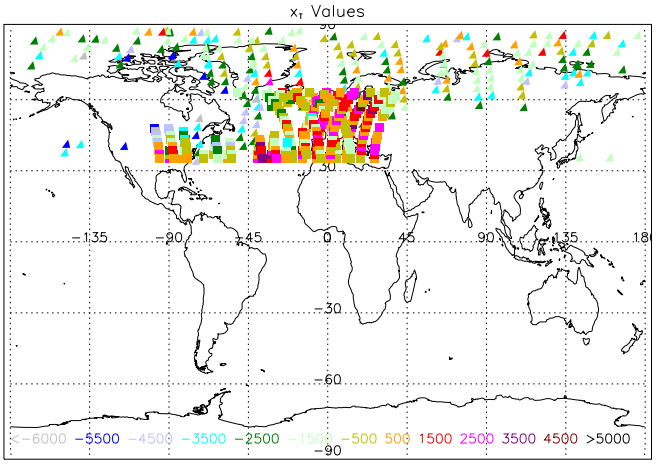

Figure 5.6 x_T values calculated using the two-level non-linear retrieval method

No clear region of increased NO_2 from aircraft can be seen, although there appear to be a greater proportion of higher x_T values over Europe than at higher latitudes.

However, there is not sufficient evidence for any firm conclusions to be made.

6 Conclusions and Further Work

It is unfortunate that the MIPAS Aircraft Emission mode data available was from such an active part of the atmosphere and from such a perturbed region. Partly due to these factors, detection of the chemical impact of commercial jet aircraft on the upper troposphere/lower stratosphere (UTLS) was not achieved. However, the difficulties that these things caused highlight the fact that it is always necessary to run a full retrieval for each atmospheric case – it isn't practical to just try a quick two-level retrieval using precomputed spectra as attempted in this project.

Assuming that retrievals of temperature, pressure, H_2O, and all other relevant gases have been completed, so that the RFM spectra actually match the real atmosphere except for the NO_2 lines which we want to use, the theory presented indicates that detection of aircraft emitted NO_2 in the UTLS is possible.

Further work might include investigating whether any of the other gases in aircraft emissions (such as CO) would be detectable using the same methods, and perhaps whether observation of changes in O_3 concentration in the UTLS would be a viable method of detecting increasing or decreasing emissions. Also, additional investigation into exactly which aspects of the weather system were causing such large variation in radiances between MIPAS spectra might be useful.

An extension to this project might include a study of the radiative impact due to aircraft by investigating contrails and cirrus formation in the UTLS.

Appendix A

RFM Driver Table

```
! RFM Driver Table for Reference Spectra
*HDR  !Text written into headers of all
      !output files
  RFM Spectra all gases included
*FLG  !List of RFM Option Flags
  RAD ILS JAC FOV CTM PTH
*SPC  !Spectral Range/Resolution
  C 1580 1750 0.0625
*GAS  !List of absorbing species
  CO2 CH4 N2O NO2 O3 HNO3 H2O SO2 NO CO
*ATM  !List of atmospheric profiles
  ../rfm_files/hgtnom.atm
  ../rfm_files/ngt.atm
*TAN
  10 11.5 13 14.5 16 18
*JAC
  8.5 11.5 14.5 200
*ILS
  ../rfm_files/ofm_16.ils
*FOV
  /home/crun/eodg/rfm/rfm_files/fov $
  /rfm_1km5.fov
*HIT
  ../rfm_files/hitran_2000.bin
*END
```

Figure A.1 Typical RFM driver table with all major infrared emitters included. Comments are preceded by exclamation marks (!)

The *FLG section shows that we want to write files containing radiance spectra (RAD flag), that we want to perform a spectral convolution with the Instrument Line Shape (ILS flag), that Jacobians (weighting functions) are to be calculated (JAC flag), that a Field-of-View convolution is being applied (FOV flag), that continuum-like features associated with H_2O and CO_2 are being taken into account (CTM flag), and that we want to create a file containing ray path diagnostics (PTH flag). The *SPC section identifies the wavenumber region which is of interest for the NO_2 emission spectrum, and specifies the resolution to be used. The *GAS section identifies the gases to be used in the simulation, while the *ATM section gives the file locations of the atmospheric profiles to be used. These files contain the pressure, temperature and molecule concentration data, as a function of altitude. Tangent heights are listed under *TAN, and *JAC specifies the heights for which Jacobians are to be calculated. *ILS gives the location of Instrument Line Shape data. The *FOV section ensures the Field-of-View (FOV) convolution is included for the finite size of the interferometer optics. The *HIT section is included as all the molecules I use are HITRAN 'line' molecules.

References

1. Grewe, V., M. Dameris, R. Hein, I. Köhler, and R. Sausen (1999), Impact of future subsonic aircraft NO_x emissions on the atmospheric composition, *Geophys. Res. Lett.*, *26*(1), 47–50.
2. Poellot, M.R., Arnott, W.P., Hallett, J., 1999. In situ observations of contrail microphysics and implications for their radiative impact. Journal of Geophysical Research (Atmospheres) 104 (D10), 12077-12084.
3. Airbus, 1997: Confirming very large demand. In: Global Market Forecast 1997-2016. Airbus Industrie, Toulouse, France, 27 pp.
4. Penner, J. E., Lister, D. H., Griggs, D. J., Dokken, D. J., and Mc-Farland, M. (Eds.): Aviation and the Global Atmosphere, Cambridge Univ. Press, New York, 1999.
5. Emmons, L.K., M.A. Carroll, D.A. Hauglustaine, G.P. Brasseur, C. Atherton, J. Penner, S. Sillman, H. Levy II, F. Rohrer, W.M.F. Wauben, P.F.J. van Velthoven, Y. Wang, D.J. Jacob, P. Bakwin, R. Dickerson, B. Doddridge, C. Gerbig, R. Honrath, G. Hubler, D. Jaffe, Y. Kondo, J.W. Munger, A. Torres, and A. Volz-Thomas, 1997: Climatologies of NO_x and NO_y: a comparison of data and models. *Atmospheric Environment*, **31,** 1851-1903
6. Brasseur, G. and Solomon, S.: Aeronomy of the middle atmosphere (third edition), Atmos. Oceanograph. Sci. Lib., p. 336 ff, Springer, Dordrecht, The Netherlands, 2005.
7. MIPAS: http://envisat.esa.int/handbooks/mipas/
8. Apodisation: http://envisat.esa.int/handbooks/mipas/CNTR2-4-4.htm
9. Kleinert, A., Aubertin, G., Perron, G., Birk, M., Wagner, G., Hase, F., Nett, H., and Poulin, R.: MIPAS Level1B algorithms overview: operational processing and characterization, Atmos. Chem. Phys. Discuss., 6, 10 673–10 711, 2006.
10. Raspollini, P., Belotti, C., Burgess, A., Carli, B., Carlotti, M., Ceccherini, S., Dinelli, B. M., Dudhia, A., Flaud, J.-M., Funke, B., Höpfner, M., López-Puertas, M., Payne, V., Piccolo, C., Remedios, J. J., Ridolfi, M., and Spang, R.: MIPAS level 2 operational analysis, Atmos. Chem. Phys., 6, 5605–5630, 2006.
11. RFM: http://www.atm.ox.ac.uk/RFM/
12. ANCAT/EC, 1995: A Global Inventory of Aircraft NO_x emissions, pp 20
13. Greenhough ,J., J.J. Remedios, H. Sembhi and L.J. Kramer, Towards cloud detection and cloud frequency distributions from MIPAS infra-red observations, Adv. Space Res, 36, 5, 800-806, 2005.
14. Kiefer, M., T. von Clarmann, U. Grabowski, M. De Laurentis, R. Mantovani, M. Milz, and M. Ridolfi: Characterization of MIPAS elevation pointing, Atmos. Chem. Phys., 7, 1615–1628, 2007